Metal-insulator transition in epitaxial VO_{2} thin films on TiO_{2} (100)

Xing Zhong, P. LeClair, Sanjoy K. Sarker, and Arunava Gupta

Phys. Rev. B **86**, 094114 — Published 26 September 2012

DOI: 10.1103/PhysRevB.86.094114

The metal-insulator transition in epitaxial VO_2 thin films on TiO_2 (100)

Xing Zhong,[1,2] P. LeClair,[1,2,*] Sanjoy K. Sarker,[2] and Arunava Gupta[1,3]

[1]*MINT Center, University of Alabama, Tuscaloosa AL 35405*
[2]*Department of Physics and Astronomy, University of Alabama, Tuscaloosa AL 35405*
[3]*Department of Chemistry and Department of Chemical and Biological Engineering, University of Alabama, Tuscaloosa AL 35405*

(Dated: August 31, 2012)

We performed detailed resistivity and impedance spectroscopy studies of epitaxial (100) VO_2 films. As the metal-insulator transition (MIT) is approached from below, the dielectric constant collapses concomitantly with a sharp increase in conductivity, revealing the coexistence of metallic and insulating phases. At lower temperatures transport in the insulating phase can be explained by small polaron hopping, with an activation scale significantly smaller than the semiconducting gap. We propose that closer to the MIT transport is dominated by polarons tunneling between metallic regions. Our results stress the critical importance of the metal-insulator phase coexistence and electronic motion coupled with ionic displacement in determining the transport behavior.

PACS numbers:

The temperature driven metal-insulator transition (MIT) of VO_2 is still the subject of intense debate, even fifty years after its discovery.[1] VO_2 exhibits an ultrafast[2] reversible metal-insulator transition (MIT) at $T_{\rm MI} \sim 341\,{\rm K}$ in the bulk, transforming from a low-temperature insulating monoclinic "M_1" phase ($P2_1/c$) to a high-temperature metallic rutile "R" phase ($P4_2/$ mnm).[3,4] At the MIT, the resistivity of VO_2 can change by a factor of as much as 10^5, accompanied by a large change in infrared reflectivity. However, a complete microscopic understanding of the MIT is still lacking, hindering the potential of VO_2 for nanoelectronics applications.[5,6]

The important physical feature of the M_1 phase in comparison to the R phase is a dimerization of V ions along the c axis, with V-V dimers tilting out of the axis.[3] The resulting doubling of the unit cell should open a gap, which led to suggestions that the insulating M_1 phase is a Peierls insulator.[3,4] This viewpoint is not wholly satisfactory: for instance, compression along c decreases $T_{\rm MI}$, contrary to what is expected of a Peierls insulator.[1] Further, recent experimental[7–10] and theoretical work[4,11] has shown that correlations are substantial in the M_1 phase, suggesting that VO_2 is close to being a Mott-Hubbard insulator. The nearby M_2 phase (stabilized by doping or pressure) is indeed a Mott insulator.[12] Belozerov et al.[13] have recently suggested that the M_1 phase is a correlated band insulator in the Peierls scenario, enhanced by intersite correlation effects on the V dimers. Probably it is best to consider the M_1 phase a dimerized Mott insulator, since apparently both dimerization and strong Coulomb correlations play crucial roles.[11,13]. In some sense, a debate over Mott-Hubbard versus Peierls merely distracts from more direct questions: what are the low-energy excitations that determine the properties of the insulator, and what is the fundamental character of the transport in the insulating phase? In this paper, we attempt to shed light on these issues by illustrating the key role of metal-insulator phase coexistence and suggesting the importance of ionic motion in determining transport behavior.

In recent years, another intriguing aspect of VO_2 has been revealed, namely nanoscale electronic phase separation,[10,14–17] the presence of persistent metallic domains within the insulating state.[18,19] These domains grow and coalesce as $T_{\rm MI}$ is approached from below, leading to a MIT by a process analogous to percolation.[9] The experimentally well-established coexistence of metallic and insulating phases[9,10] is typically omitted in descriptions of transport. It seems reasonable that any model of conductivity near the MIT must take into account this phase coexistence. Further, the small energy barriers to switching ($\sim 80\,{\rm K}$)[19]) suggest that dynamic metallic regions should be present well below $T_{\rm MI}$, impacting the conductivity over a broad temperature range. Zylbersztejn and Mott proposed long ago[4] that at low temperature conductivity is due to hopping between localized impurity states, whereas at higher temperature it has the activated form characteristic of an intrinsic semiconductor. Here, we argue that the situation is essentially reversed.

It has become customary to fit the conductivity in the M_1 phase within a small region below T_{MI} to an activated form, $\ln\sigma \propto -\Delta/k_BT$. Indeed, electronic structure calculations[11,20] suggest that the M_1 phase is a semiconductor, with a charge gap $\Delta_c \approx 0.6\,{\rm eV}$. One must caution, however, that since transport measurements are typically restricted to a narrow temperature range, within a few tens of kelvin of $T_{\rm MI}$, the data can easily be fitted to other forms. Moreover, metallic domains should play the dominant role in transport in this regime, and the semiconductor model can not explain their presence. What data does exist at lower T has often been interpreted as characteristic of variable-range hopping (VRH).[21,22] The presence of VRH is exceedingly unlikely, since VRH occurs between Anderson-localized states in a strongly disordered system. In such a system the spectrum is gapless, and the lattice translational symmetry is explicitly broken. Further, it is unclear why VRH-like conductivity

should be seen even in high quality single crystals and epitaxial films,[4] which lack the requisite quenched disorder. To obtain a better understanding of the transport properties at low temperature and the origin of metallic domains near $T_{\rm MI}$ it is necessary to carry out measurements on a relatively clean system over a broad temperature range.

In this work, we report detailed resistivity and impedance spectroscopy studies of epitaxial (100) VO_2 films down to 80 K. Impedance spectroscopy reveals both insulating and metallic characteristics in the region surrounding the MIT, indicating clearly that the established phase coexistence plays an important role in determining transport. Moreover, the frequency-dependent impedance can be explained by simply considering parallel contributions of a real and constant conductivity and a real dielectric constant, suggesting that phase coexistence is in fact the *dominant* factor in determining transport. More detailed studies of the temperature-dependent conductivity concurs with previous measurements of Andreev and Klimov,[23] who have suggested that over a wide temperature range the conductivity of the M_1 phase follows the form:

$$\sigma = \sigma_0 \exp\left(-\Delta_0/k_BT + k_BT/E_{ph}\right) \qquad (1)$$

They argued that the unusual T-linear term is characteristic of phonon-assisted tunneling via small polarons, and arises due to variations of ionic positions, as shown by Bryksin.[24] Our data strongly support this conjecture, and we extend their work by considering transport along the a and c axes separately. We will further argue, based on our data and microscopic considerations, that this picture has to be modified to account for the appearance metallic domains and percolation-like conductivity near the MIT. Our results and other recent discoveries raise the possibility that VO_2 belongs to a new class of correlated semiconductors, in which the physics is governed by new type of intrinsic excitations which involve electronic motion strongly coupled with ionic displacement.

We prepared epitaxial VO_2 thin films on TiO_2 (100) substrates (5×5 mm from CrysTec, cleaned by acetone and isopropanol) using a home-built hot wall low pressure chemical vapor deposition system. Vanadyl acetylacetonate (98% Sigma-Aldrich) was used as the precursor without further purification. Pure O_2 was used as the carrier gas, with a chamber pressure of 65 Pa. During deposition, the substrate was maintained at 663 K, the chamber walls at 443 K and the precursor at 413 K. The deposition rate was $\sim$2–2.5 nm/min. The thicknesses of the films were determined by X-ray reflectivity, and crystallographic quality was ascertained by X-ray diffraction (XRD), both in a Philips X'Pert system with Cu K-α ($\lambda=0.154$ nm) radiation.

Figure 1a shows a room temperature x-ray diffraction θ–2θ scan for VO_2 films of varying deposition times grown on TiO_2 (100) substrates. At room temperature the films are in the monoclinic M_1 phase, and only (200) and (400)

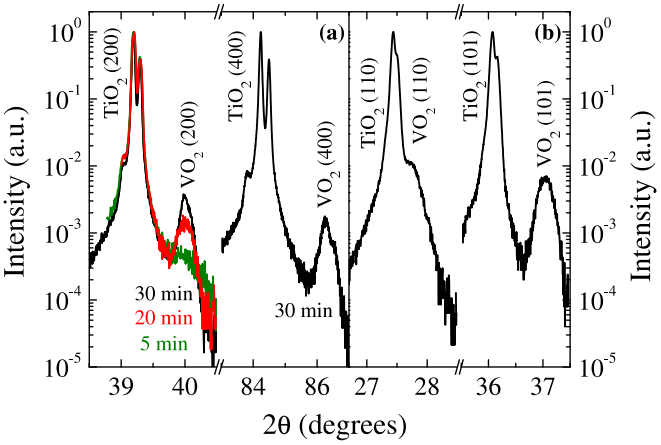

FIG. 1: XRD pattern using Cu K-α radiation of **(a)** VO_2 films with different deposition times (thicknesses from 15 – 75 nm) showing the TiO_2 rutile (200) and (400) peaks and VO_2 quasi-rutile (200) and (400) peaks. **(b)** (110) and (101) quasi-rutile peaks for a 75 nm VO_2 (100) when the sample is tilted to the corresponding planes. No peaks were observed for 2θ angles not shown.

VO_2 peaks are observed, suggesting that the films are epitaxial and phase pure with a (100) orientation. We refer to the VO_2 peaks by their quasi-rutile (200) and (400) indices, though strictly for the monoclinic phase they are (020) and (040). The peak positions do not vary with thickness, suggesting strain does not change significantly in this thickness range, and peak widths imply in-plane coherence lengths approximately equal to film thicknesses. Diffraction from the VO_2 quasi-rutile (110) and (101) planes when the film is tilted the appropriate angle are also shown in Fig. 1b. From these results, for a 75 nm VO_2 film the out-of-plane lattice parameter is $a=0.451\pm0.002$ nm, contracted by $-0.9\pm0.4\%$, while the in-plane lattice parameters are $b=0.457\pm0.002$ nm and $c=0.289\pm0.002$ nm, indicating an expansion of $+0.4\pm0.1\%$ along b and $1.0\pm0.7\%$ along c. Compression along a and expansion along b and c is consistent with the lattice mismatch with the TiO_2 substrate (+0.82% along b, +3.5% along c).

In addition, the epitaxial growth of the VO_2 films was confirmed by measuring the TiO_2 and VO_2 (101) peaks as a function of φ, as shown in Fig. 2 for a 30 nm VO_2 sample. The φ scan indicates two-fold in-plane symmetry for both film and substrate, as expected. The full-width at half maximum (FWHM) is $\approx 0.4-0.5^\circ$, indicating the presence of a highly epitaxial VO_2 film. The surface morphology of the films was studied using atomic force microscopy (Digital Instruments Nanospec-4), showing elliptical domains with major axes parallel to the TiO_2 c-axis. The mean grain size increased with film thickness, indicative of an island growth mode, and surface roughness ranges from 0.6 nm (15 nm film) to 3.1 nm (75 nm film).

Four point probe dc transport measurements were carried in a liquid nitrogen cryostat and a physical prop-

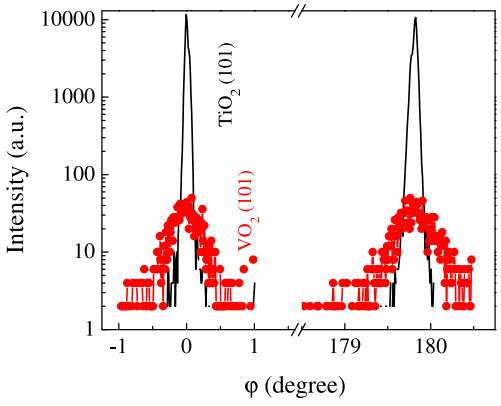

FIG. 2: φ scan of the $TiO_2(101)$ and $VO_2(101)$ peaks for a 75 nm sample. The peaks have a full-width at half maximum of $0.4-0.5^\circ$. No peaks are observed for φ angles not shown.

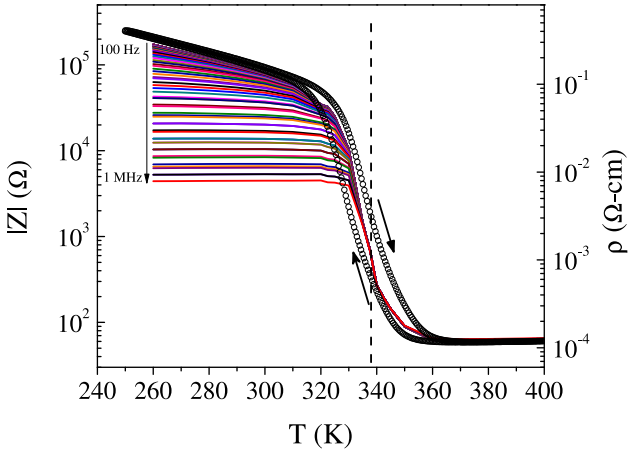

FIG. 3: dc resistivity (symbols) and impedance from 100 Hz to 1 Mhz (lines) as a function of temperature for a 75 nm-thick VO_2 (100) film along the c-axis. The dc measurement was performed by a four-point probe method, in both heating and cooling, and the impedance measurements by a two-point probe method in heating. The vertical line indicates the metal-insulator transition temperature.

erty measurement system (PPMS, Quantum Design). Impedance measurements (magnitude $|Z|$ and phase θ) were performed using a two-point probe method with a HP-4284A LCR meter in the same cryogenic systems for a 75 nm thick film. The measurements were performed with increasing measurement temperature (0.5 K/min) from $T = 250-360$ K for frequencies $f = 10^2 - 10^6$ Hz. In order to be certain that the impedance measurements reflected the film alone, the series resistance and inductance from the cabling was measured and found to provide a negligible contributions under all conditions. Figure 3 shows the dc resistivity ρ and the magnitude of the impedance $|Z|$ at different frequencies as a function of temperature. Above the metal-insulator transition (MIT), little variation with frequency is observed, while below the metal-insulator transition $|Z|$ decreases rapidly with increasing frequency. We determined $T_{\rm MI}$ from $\rho_{\rm dc}$ to be 338 ± 1 K,[25] only slightly below the bulk value.[3] Figure 4(a,b) shows the real (Z') and imaginary (Z'') components of the impedance as a function of f for temperatures above and below $T_{\rm MI}$.

In order to extract the conductivity and dielectric functions, and in light of the metal-insulator phase coexistence, we modeled the film as an effective medium with parallel contributions of a real conductivity $\sigma(f)$ and a real dielectric function $\epsilon(f)$. Assuming an effective medium of length d and cross-sectional area A, this gives

$$Z'(f) = \left(\frac{d}{A}\right) \frac{\sigma(f)}{\sigma^2(f) + 4\pi^2 f^2 \epsilon^2(f)}$$
$$Z''(f) = \left(\frac{d}{A}\right) \frac{-2\pi i f \epsilon(f)}{\sigma^2(f) + 4\pi^2 f^2 \epsilon^2(f)} \qquad (2)$$

One can then find the frequency-dependent conductivity and dielectric function in terms of the measured real and imaginary parts of the impedance, or the impedance magnitude and phase angle:

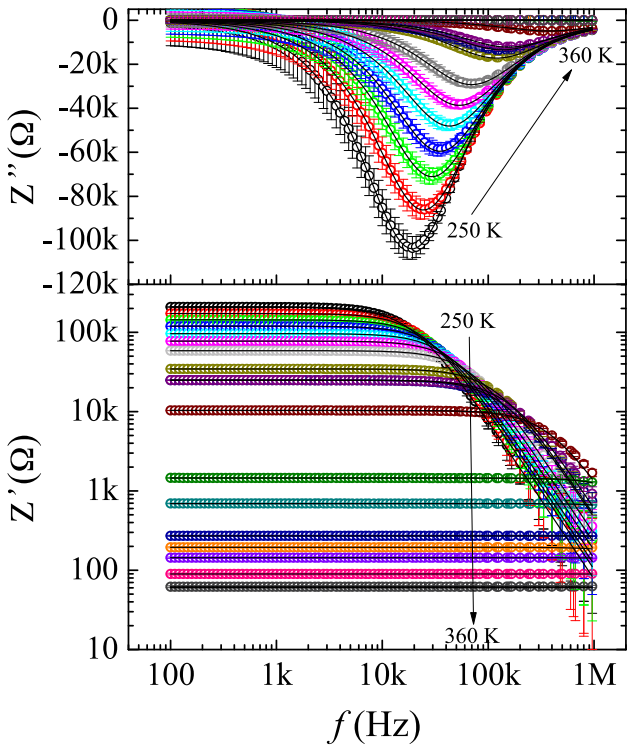

FIG. 4: Real and imaginary components of the impedance (symbols), along with fits (lines) to an effective media model with frequency-independent σ and ϵ (see text). Measurements were performed while warming the sample, at temperatures of 250, 260, 270, 280, 290, 300, 310, 320, 322.5, 325, 330, 335, 337.6, 340, 342.5, 345, 350, and 360 K.

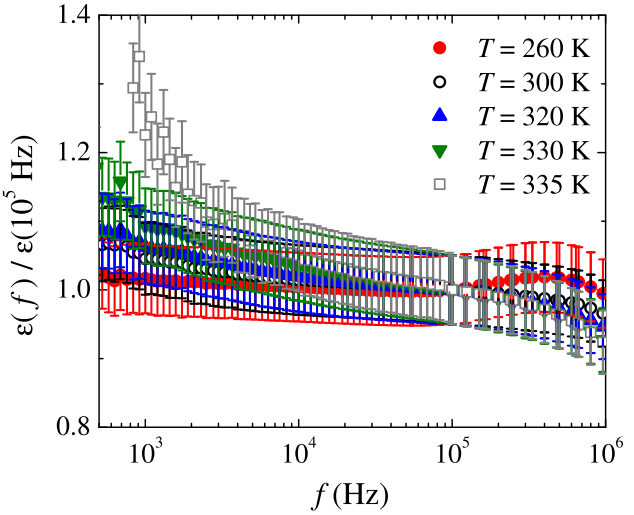

FIG. 5: Normalized dielectric function versus frequency resulting from a fit of the impedance data to a parallel $\epsilon(f)$-$\sigma(f)$ model (see text), normalized to 100 kHz, at various temperatures. The error bars represent uncertainties in ϵ due to the uncertainty in the magnitude of the impedance, phase angle, and frequency.

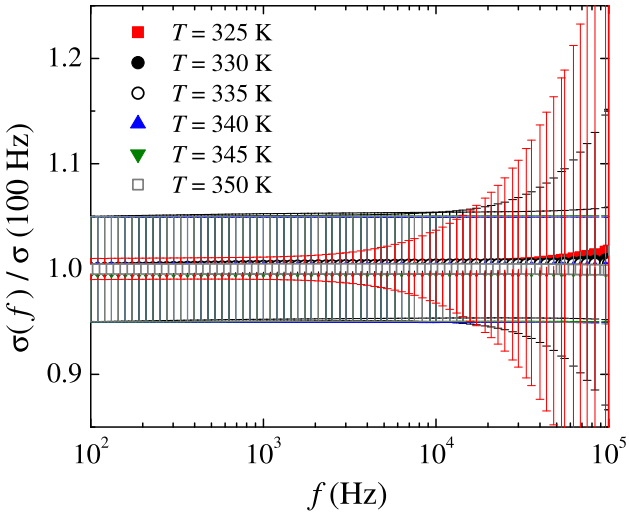

FIG. 6: Conductivity versus frequency resulting from a fit of the impedance data to a parallel $\epsilon(f)$-$\sigma(f)$ model (see text), normalized to 100 Hz, at various temperatures. The error bars represent uncertainties in σ due to the uncertainty in the magnitude of the impedance, phase angle, and frequency.

$$\epsilon(f) = -\frac{Z''}{2\pi f|Z|^2}\left(\frac{d}{A}\right) = -\frac{\sin\theta}{2\pi f|Z|}\left(\frac{d}{A}\right)$$
$$\sigma(f) = \frac{Z'}{|Z|^2}\left(\frac{d}{A}\right) = \frac{\cos\theta}{|Z|}\left(\frac{d}{A}\right) \quad (3)$$

Using our measured $Z'(f)$ and $Z''(f)$, we calculated $\epsilon(f)$ and $\sigma(f)$ at each measurement temperature (up to the overall geometrical factor d/A). However, we found that the extracted $\sigma(f)$ and $\epsilon(f)$ showed little change with $f \leq 1$ MHz at a given temperature. Figure 5 shows the dielectric function $\epsilon(f)$ extracted at temperatures below the MIT, along with propagated uncertainties in ϵ due to the measurement uncertainties in $|Z|$, θ, and f (see Appendix). Over frequency ranges and temperatures where $\epsilon(f)$ can be meaningfully extracted, the frequency variation is within the experimental uncertainties. At temperatures well above the MIT, uncertainty allows no meaningful extraction of $\epsilon(f)$; the same is at any temperature for frequencies below $f \lesssim 1$ kHz. Similar conclusions hold for the $\sigma(f)$ data, shown in Fig. 6. In particular for $\sigma(f)$, the uncertainty is too large to extract $\sigma(f)$ reliably at temperatures well below the MIT or frequencies above $f \sim 100$ kHz at any temperature. Also, as one would expect, the uncertainty in $\sigma(f)$ grows substantially at higher frequencies.

Returning to the impedance data, plots of Z' and Z'' versus frequency are only one way to represent the data. Another common (but essentially equivalent) method of visualizing impedance data is using a Nyquist plot of Z'' versus Z'. In this representation, a parallel combination of frequency-independent σ and ϵ should yield a semicircular plot. In Fig. 7 we show Nyquist plots of the

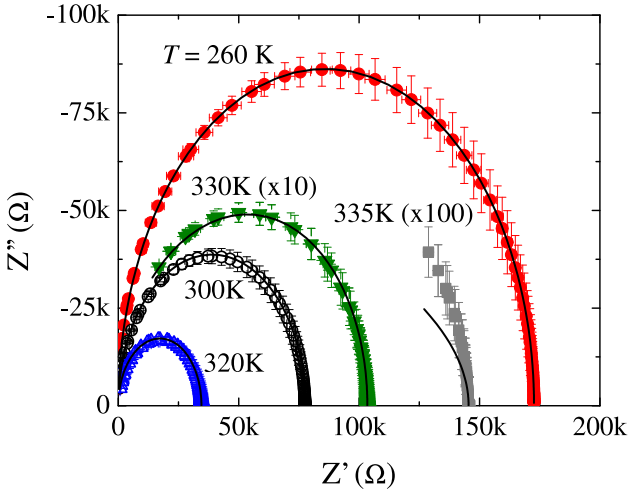

FIG. 7: Nyquist plot of the impedance data (symbols) at various temperatures. Note that the $T = 330$ K data has been multiplied by 10 for both axes, and the $T = 335$ K data by 100 for both axes. The solid lines are the same fits from Fig. 4.

impedance data at several temperatures below the MIT. Semicircular characteristics are observed, consistent with our conclusions from modeling the $Z'(f)$ and $Z''(f)$ data. At temperatures close to and above the MIT ($T \gtrsim 340$ K), the imaginary portion of the impedance is sufficiently small in the frequency range studied that the plot is essentially reduced to a cluster of points near the Z' axis. This is further indicative of the nearly Ohmic behavior of the films well above the MIT.

The negligible variation of $\epsilon(f)$ or $\sigma(f)$ suggests that we are justified in treating both as *frequency-independent* for $f \lesssim 1$ MHz. In this case, both σ and ϵ can be ex-

tracted at any temperature readily. (We caution that this is demonstrably *not* true at higher frequencies, see for example the optical conductivity in reference 9.) Assuming a *frequency-independent* σ and ϵ, with an effective medium of length d and cross-sectional area A, Z' and Z'' are given by

$$\begin{aligned} Z'(f) &= R/(1+4\pi^2 f^2\tau^2) \\ Z''(f) &= -2\pi f\tau R/(1+4\pi^2 f^2\tau^2) \end{aligned} \quad (4)$$

with $R = d/\sigma A$ and $\tau = \epsilon/\sigma$. This is equivalent to a parallel RC circuit with $\tau = RC$ and $C = \epsilon A/d$, or a single capacitor with a complex dielectric constant, $\epsilon = \epsilon' + i\epsilon'' = \epsilon' + i\sigma/2\pi f$. Within this model, the Nyquist plot should be a semicircle centered on $(R/2, 0)$ with radius R:

$$\left(Z' - \frac{R}{2}\right)^2 + (Z'')^2 = \left(\frac{R}{2}\right)^2 \quad (5)$$

The intercept along the real axis should thus be twice the intercept along the imaginary axis, consistent with our data in Fig. 7. Fits to this model are shown as lines in Fig. 4 and Fig. 7, and excellent agreement is found at all temperatures. Only the $Z'(f)$ and $Z''(f)$ data were fit (Fig. 4), the same fit data are shown in Fig. 7. Moreover, in this case, ϵ and σ can be reliably more extracted taking into account experimental uncertainties at any temperature. The values of R, τ, σ, and ϵ from fits to Eqs. 4 as a function of temperature are shown in Fig. 8. The fitted σ and R agree well with the measured dc resistivity ρ_{dc}. The parameter τ may be interpreted as a relaxation time, and exhibits a dramatic collapse as the film enters the metallic state. Well below the MIT, ϵ is roughly constant, while well above the MIT we find $\epsilon = 0$ taking into account propagated uncertainties. Over the same temperature range, σ rises rapidly; taken together, this points clearly toward the percolative nature of the MIT.[9] Around the MIT, ϵ rises sharply,[9] though we caution that in the same region the propagated uncertainty in ϵ increases commensurately.

In order to further clarify the nature of the transport near and well below the MIT, as well as elucidate any anisotropy with respect to crystallographic axes, we also measured the resistivity films patterned into strips oriented along the a or c axes. We patterned 75 nm VO_2 films into strips oriented with their length along the a or c axis using standard lithographic techniques for low temperature transport measurements. The c-axis-oriented strips were 50 μm wide, 500 μm long, while the a-axis-oriented strips 20 μm wide, 366 μm long. Figure 9 shows the resistivity of a- and c-axis oriented structures as a function of temperature. While the overall behavior is qualitatively similar, the change in resistance across the metal-insulator transition is much stronger for c-axis oriented structures. However, whether the strong anisotropy in the resistivity (particularly above the MIT) arises from micro- cracks along the c-axis or is an intrinsic property of VO_2 is still unclear.

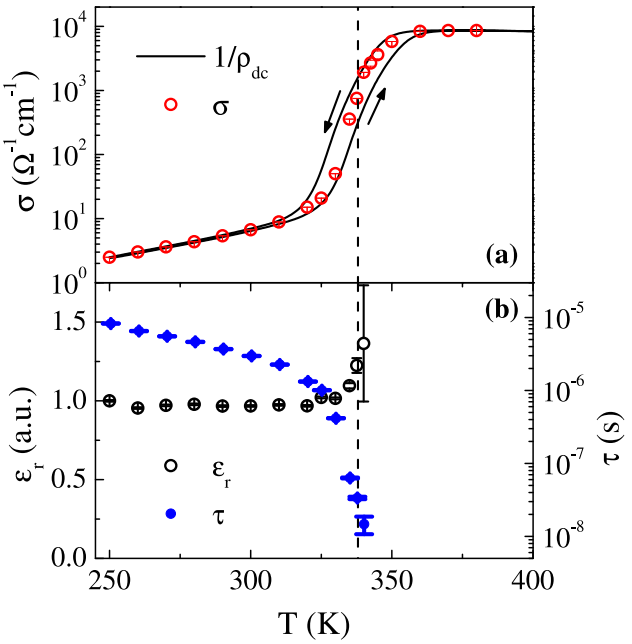

FIG. 8: **(a)** Conductivity $\sigma(T)$ extracted from fitting frequency-dependent impedance spectra (see text) compared to the inverse of the measured dc resistivity $1/\rho_{dc}(T)$. The conductivity has been normalized to agree with ρ_{dc} at 250 K. The MIT is denoted by a dashed vertical line. **(b)** Dielectric constant ϵ and relaxation time $\tau = \epsilon/\sigma$ extracted as a function of temperature.

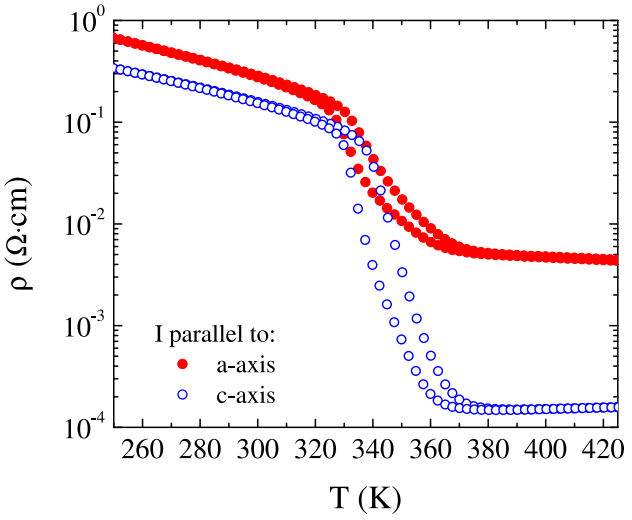

FIG. 9: Resistivity of strips patterned along the a and c axes (see text) as a function of temperature.

The upper inset of Fig. 10 shows $\ln\rho$ versus $1/T$ along both a and c axes from $T = 80 - 300$ K. One is tempted to fit the conductivity in this regime to activated behavior, which neglects the role of the metallic domains and whose presence precludes such intrinsic behavior. The

data in Fig. 10 clearly reveal that activated behavior is plausibly followed only at low temperatures, and the deviation above $\sim 150\,\mathrm{K}$ is marked. This illustrates that activation energies obtained near the MIT over a limited T range will yield dubious results. This may explain the wide range of activation energies reported,[4,22] and why there is a standing question as to the transport energy scale.[9,12]

In VRH conductivity, the competition between random potential barriers and overlap integrals leads to a characteristic temperature dependence of the conductivity. In this present case, one rather expects an essentially fixed tunneling barrier height presented by the semiconducting regions while the *distance* between dynamic metallic regions fluctuates. Bryksin[24] has previously considered the effects of lattice vibrations on the probability of small polaron hopping. In this model, similar to earlier work of Hurd[26] and applied to VO_2 by Andreev and Klimov[23], the conductivity follows

$$\sigma = \frac{e^2\pi^{3/2}na^2I^2}{2h\sqrt{\Delta_0}\,(k_BT)^{3/2}}\exp\left(-\frac{\Delta_0}{k_BT}+\frac{k_BT}{E_{ph}}\right) \qquad (6)$$

where n is the carrier concentration, a the lattice spacing, I the overlap integral between hopping sites, e the electron charge, h Planck's constant, and Δ_0 and E_{ph} are the activation and vibrational energy scales, respectively. One can eliminate the temperature-dependent prefactor (reflecting a variation in carrier density) in Eq. 6 by plotting $\ln(\sigma T^{3/2}) = k_BT/E_{ph} - \Delta_0/k_BT + (\mathrm{const})$. This is shown in Fig. 10 for both a and c axis data, along with a fit to Eq. 6 which describes the data remarkably well over a substantial region below T_{MI}. From this, we extract $\Delta_0 \approx 107 \pm 1\,\mathrm{meV}$ and $E_{ph} \approx 3.4 \pm 0.1\,\mathrm{meV}$ for the c axis, and $\Delta_0 \approx 101 \pm 1\,\mathrm{meV}$ and $E_{ph} \approx 5.6 \pm 0.1\,\mathrm{meV}$ for the a axis, in agreement with reference 23. Note that at the onset of the MIT, deviation from Eq. 6 is rapid (lower inset to Fig. 10).

There are three crucial features to note. (1) Activated behavior is recovered at lowest temperatures, but the activation energy is far below the charge gap ($\Delta_0 \ll \Delta_c$), which suggests that conduction involves electronic states inside the gap. The activation energy Δ_0 is essentially independent of crystallographic orientation, as expected. (2) With increasing T, $\ln(\sigma T^{3/2})$ becomes linear in T. The relevant scale E_{ph} is now much smaller, characteristic of phonons, and consistent with the significantly different values of E_{ph} obtained for a- and c-axis transport. This is also compatible with the polaronic picture of Bryksin, Andreev, and Klimov (BAK). (3) However, important physics is still missing, since above about 320 K there is a sharp deviation from the BAK model (Eq. 6), with σ rising much more rapidly just before and as the MIT begins. This can be attributed to the appearance of metallic domains, leading to percolation-type conductivity.[9,19] These properties suggest that there are intrinsic excitations within the semiconducting gap.

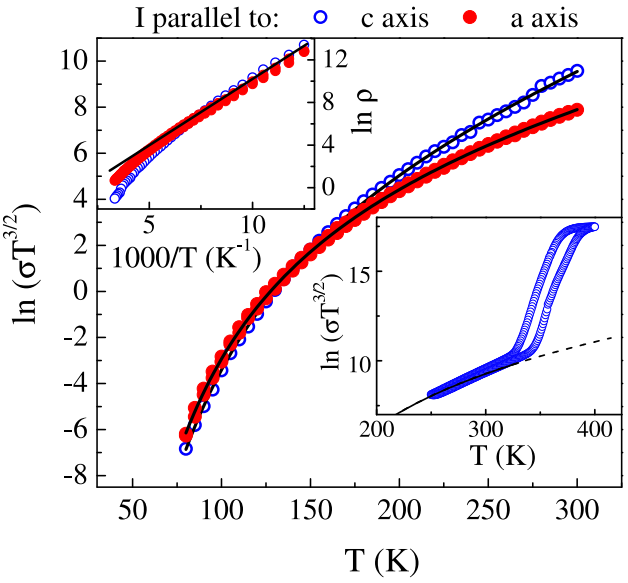

FIG. 10: $\ln(\sigma T^{3/2})$ versus T along the a and c axes. The solid lines are fits to the data using the BAK model (see text).[23] **Lower inset:** $\ln(\sigma T^{3/2})$ versus T near the transition, with the same fitting line. **Upper inset:** $\ln\rho$ versus $1/T$, showing that activated behavior is approximately followed only at low temperatures.

Considering percolation-type transport through the MIT, in the simplest approximation one may treat the transport as a two-channel parallel circuit. We consider a rutile phase channel of conductivity $\sigma_r(T)$ and volume fraction x_r and a monoclinic phase channel of conductivity $\sigma_m(T)$ and volume fraction $1-x_r$, giving rise to a total dc conductivity $\sigma(T)$:

$$\sigma(T) = \sigma_m(T) + x_r\,[\sigma_r(T) - \sigma_m(T)] \qquad (7)$$

Using the aforementioned BAK model (Eq. 6) for the monoclinic phase conductivity $\sigma_m(T)$, and a linear approximation for the metallic rutile conductivity $\sigma_r(T)$, we may estimate the rutile volume fraction x_r at any temperature by fitting the measured conductivity to Eq. 7.[27] As noted previously,[27] a simple-minded but successful approach is to empirically treat the phase co- existence near the MIT as a first-order chemical equilibrium,

$$x_r = \frac{1}{1+\exp\left(\frac{\Delta E_1 - T\Delta E_2}{k_BT}\right)} = \frac{\sigma(T)-\sigma_m(T)}{\sigma_r(T)-\sigma_m(T)} \qquad (8)$$

where $\Delta E_1 - T\Delta E_2$ is a free-energy-like term. Figure 11 shows the rutile volume fraction x_r as a function of temperature, extracted from fitting the conductivity versus temperature in both heating and cooling. We find $E_1 \sim 2.5\,\mathrm{eV}$ for both heating and cooling, while $\Delta E_2 \sim 6.7\,\mathrm{meV/K}$ on heating and $\Delta E_2 \sim 7.0\,\mathrm{meV/K}$ on cooling. The calculated metallic fraction x_r remains significant well below the MIT, in agreement with earlier

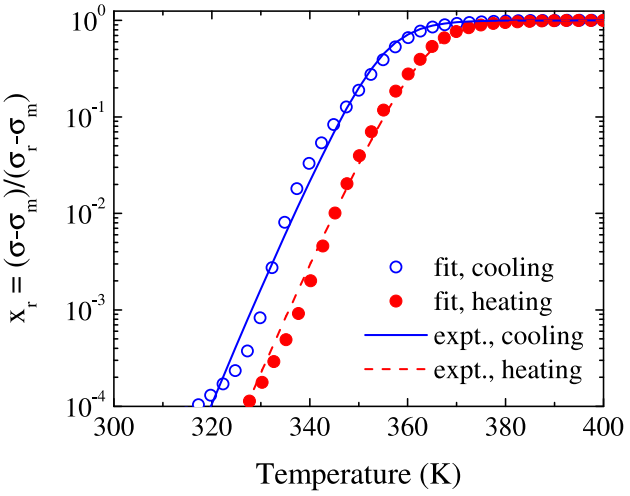

FIG. 11: Metallic rutile phase fraction x_c deduced from fitting the conductivity versus temperature (see text).

measurements.[17–19] Though we do not wish to take this clearly over-simplified model too seriously, one must conclude that even in the simplest of models the metallic and semiconducting phases coexist over a wide range of temperatures, with significant influence over transport properties.

We now *speculate* on the possible microscopic origin of these excitations. The electronic properties of VO_2 can be described in terms of 3 low- lying d orbitals of the V atom which share one electron: an e_g^π doublet and a lower energy a_{1g} level[4,11]. We can assume that the ionic potential energy has local minima for a V ion at the dimer M_1 sites, and also at rutile R sites at a higher energy. Electronic properties are usually calculated by freezing the ions at the local minima of a particular phase,[11,20]. The $e_g^\pi - a_{1g}$ splitting is small in the rutile (R) site, leading to a metal, as the 3 bands overlap at the Fermi level. This splitting is larger in the M_1 phase, creating a half-filled, one-band dimerized Hubbard model based on the lower a_{1g} level. Dimerization and correlation effects then open a gap, creating an insulator[11,20]. The electron is essentially localized within the dimer, as the inter-dimer hopping is quite small. An added electron will go into the empty e_g^π bands, separated by $\Delta_c \sim 0.6eV$ from the occupied band. This rigid semiconductor model clearly cannot explain the observed transport.

However, the energy cost Δ_0 should be lower ($< \Delta_c$) if the added electron goes into an interstitial region and polarizes the medium. Such a polaron would hop from site to site, giving rise to BAK-like conductivity at low T. Another type of excitation is obtained by moving a V ion (along with its electron) from the dimer to its local minimum near the R site, thus creating a metallic R ion. Such defects are always generated thermally in ionic crystals. In VO_2, there should be an *effective attraction* between these metallic ions, which would favor domain formation since electrons localize easily within a metallic domain, thereby lowering their hopping energy considerably. Another reason for clustering is that energy cost of creating two isolated R ions is twice the energy needed to create two neighboring ones by breaking a single dimer. At low T, the conduction is expected to be due to polarons tunneling between isolated small clusters. With increasing T clusters will grow in size, coalesce and percolate, leading to the MIT. We stress that these arguments are only qualitative, but seem quite plausible and will hopefully point the way to a more complete theory of the metal-insulator transition in VO_2.

We have shown, in agreement with recent experiments,[10,14–19] that over a broad temperature range near the VO_2 metal-insulator transition, the metallic and insulating phases coexist. By performing impedance spectroscopy on single crystalline films, we clearly establish that an explanation of transport must include this phase coexistence. Moreover, the detailed temperature dependence of transport well below the transition reveals two important mechanisms, small polaron hopping and activated transport, important both well into the insulating regime and up to the metal-insulator transition. More generally we have speculated, based on microscopic considerations, that standard pictures of correlated transport have to be modified to account for the appearance metallic domains near a metal-insulator transition. Our results and other recent discoveries raise the possibility that VO_2 belongs to a new class of correlated semiconductors, in which the physics is governed by new type of intrinsic excitations which involve electronic motion strongly coupled with ionic displacement. Put another way, our work suggests that in systems like VO_2, one cannot simply imagine electron transport in a fixed or thermally vibrating lattice, lattice motion and electronic motion cannot be decoupled as is typically the case.

Acknowledgments

The authors gratefully acknowledge D. Mazumdar, M. Viswanathan and H. Sims for helpful discussions, and CrysTec (Berlin) for providing high quality TiO_2 substrates. This research was supported by funding from NSF grant DMR-0706280.

* pleclair@ua.edu; http://bama.ua.edu/~pleclair

[1] F. J. Morin, Phys. Rev. Lett. **3**, 34 (1959).
[2] A. Cavalleri, T. Dekorsy, H. H. W. Chong, J. C. Kieffer, and R. W. Schoenlein, Phys. Rev. B **70**, 161102 (2004).
[3] J. B. Goodenough, J. Solid State Chem. **3**, 490 (1971).
[4] A. Zylbersztejn and N. F. Mott, Phys. Rev. B **11**, 4383 (1975).
[5] H.Jerominek, F.Picard, and D.Vincent, Opt. Eng. **32**, 209 (1993).
[6] T. Driscoll, H.-T. Kim, B.-G. Chae, M. D. Ventra, and D. N. Basov, Appl. Phys. Lett. **95**, 043503 (2009).
[7] M. W. Haverkort, Z. Hu, A. Tanaka, W. Reichelt, S. V. Streltsov, M. A. Korotin, V. I. Anisimov, H. H. Hsieh, H.-J. Lin, C. T. Chen, et al., Phys. Rev. Lett. **95**, 196404 (2005).
[8] T. C. Koethe, Z. Hu, M. W. Haverkort, C. Schüßler-Langeheine, F. Venturini, N. B. Brookes, O. Tjernberg, W. Reichelt, H. H. Hsieh, H.-J. Lin, et al., Phys. Rev. Lett. **97**, 116402 (2006).
[9] M. M. Qazilbash, M. Brehm, B.-G. Chae, P.-C. Ho, G. O. Andreev, B.-J. Kim, S. J. Yun, A. V. Balatsky, M. B. Maple, F. Keilmann, et al., Science **318**, 1750 (2007).
[10] A. Frenzel, M. M. Qazilbash, M. Brehm, B.-G. Chae, B.-J. Kim, H.-T. Kim, A. V. Balatsky, F. Keilmann, and D. N. Basov, Phys. Rev. B **80**, 115115 (2009).
[11] S. Biermann, A. Poteryaev, A. I. Lichtenstein, and A. Georges, Phys. Rev. Lett. **94**, 026404 (2005).
[12] J. P. Pouget, H. Launois, J. P. D'Haenens, P. Merenda, and T. M. Rice, Phys. Rev. Lett. **35**, 873 (1975), and unpublished results from www.lps.u-psud.fr/IMG/ppt/Pouget.ppt.
[13] A. S. Belozerov, M. A. Korotin, V. I. Anisimov, and A. I. Poteryaev, Phys. Rev. B **85**, 045109 (2012).
[14] Y. J. Chang, J. S. Yang, Y. S. Kim, D. H. Kim, T. W. Noh, D.-W.Kim, E. Oh, B. Kahng, and J. S. Chung, Phys. Rev. B **76**, 075118 (2007).
[15] A. C. Jones, S. Berweger, J. Wei, D. Cobden, and M. B. Raschke, Nano Lett. **10**, 1574 (2010).
[16] J. Kim, C. Ko, A. Frenzel, S. Ramanathan, and J. E. Hoffman, Appl.Phys. Lett. **96**, 213106 (2010).
[17] M. M. Qazilbash, A. Tripathi, A. A. Schafgans, B.-J. Kim, H.-T. Kim, Z. Cai, M. V. Holt, J. M. Maser, F. Keilmann, O. G. Shpyrko, et al., Phys. Rev. B **83**, 165108 (2011).
[18] A. Sharoni, J. G. Ramírez, and I. K. Schuller, Phys. Rev. Lett. **101**, 026404 (2008).
[19] J.-G. Ramírez, A. Sharoni, Y. Dubi, M. E. Gómez, and I. K. Schuller, Phys. Rev. B **79**, 235110 (2009).
[20] B. Lazarovits, K. Kim, K. Haule, and G. Kotliar, Phys. Rev. B **81**, 115117 (2010).
[21] K. G. West, J. Lu, L. He, D. Kirkwood, W. Chen, T. P. Adl, M. S. Osofsky, S. B. Qadri, R. Hull, and S. A. Wolf, J. Supercond. Nov. Magn. pp. 87–92 (2008).
[22] S. S. N. Bharadwaja, C. Venkatasubramanian, N. Fieldhouse, S. Ashok, M. W. Horn, and T. N. Jackson, Appl. Phys. Lett. **94**, 222110 (2009).
[23] V. Andreev and V. Klimov, Physics of the Solid State **49**, 2251 (2007).
[24] V. V. Bryksin, Sov. Phys. JETP **73**, 861 (1991).
[25] The metal-insulator transition temperature is defined as the temperature where the second derivative of the dc resistivity crosses zero on heating.
[26] C. M. Hurd, J. Phys. C.: Solid State Phys. **18**, 6847 (1985).
[27] X. Zhong, X. Zhang, A. Gupta, and P. LeClair, J. Appl. Phys. **110**, 084516 (2011).